

Doping evolution of antiferromagnetism and transport properties in nonsuperconducting $\text{BaFe}_{2-2x}\text{Ni}_x\text{Cr}_x\text{As}_2$

Rui Zhang,^{1,*} Dongliang Gong,^{1,*} Xingye Lu,¹ Shiliang Li,^{1,2} Mark Laver,³ Christof Niedermayer,³ Sergey Danilkin,⁴ Guochu Deng,⁴ Pengcheng Dai,^{5,1} and Huiqian Luo^{1,†}

¹Beijing National Laboratory for Condensed Matter Physics, Institute of Physics, Chinese Academy of Sciences, Beijing 100190, China

²Collaborative Innovation Center of Quantum Matter, Beijing, China

³Laboratory for Neutron Scattering and Imaging, Paul Scherrer Institute, CH-5232 Villigen, Switzerland

⁴Bragg Institute, Australian Nuclear Science and Technology Organization, New Illawarra Road, Lucas Heights NSW-2234 Australia

⁵Department of Physics and Astronomy, Rice University, Houston, Texas 77005, USA

(Received 27 November 2014; revised manuscript received 26 January 2015; published 12 March 2015)

We report elastic neutron scattering and transport measurements on the Ni and Cr equivalently doped iron pnictide $\text{BaFe}_{2-2x}\text{Ni}_x\text{Cr}_x\text{As}_2$. Compared with the electron-doped $\text{BaFe}_{2-x}\text{Ni}_x\text{As}_2$, the long-range antiferromagnetic (AF) order in $\text{BaFe}_{2-2x}\text{Ni}_x\text{Cr}_x\text{As}_2$ is gradually suppressed with vanishing ordered moment and Néel temperature near $x = 0.20$ without the appearance of superconductivity. A detailed analysis on the transport properties of $\text{BaFe}_{2-x}\text{Ni}_x\text{As}$ and $\text{BaFe}_{2-2x}\text{Ni}_x\text{Cr}_x\text{As}_2$ suggests that the non-Fermi-liquid behavior associated with the linear resistivity as a function of temperature may not correspond to the disappearance of the static AF order. From the temperature dependence of the resistivity in overdoped compounds without static AF order, we find that the transport properties are actually affected by Cr impurity scattering, which may induce a metal-to-insulator crossover in highly doped $\text{BaFe}_{1.7-y}\text{Ni}_{0.3}\text{Cr}_y\text{As}_2$.

DOI: [10.1103/PhysRevB.91.094506](https://doi.org/10.1103/PhysRevB.91.094506)

PACS number(s): 74.70.Xa, 75.50.Ee, 75.25.-j, 74.25.F-

I. INTRODUCTION

A determination of the complex phase diagram in high-transition (high- T_c) temperature superconductors is the first step to understand the mechanism of high- T_c superconductivity [1–4]. In iron pnictides, the parent compounds exhibit a tetragonal-to-orthorhombic lattice distortion below T_s and antiferromagnetic (AF) order below T_N . While superconductivity (SC) emerges upon sufficient electron/hole or isoelectronic doping to the parent compounds such as BaFe_2As_2 [5–8], the gradual suppression of the orthorhombic lattice distortion and AF order near optimal superconductivity suggests the presence of a quantum critical point (QCP) hidden beneath the superconducting dome, which may be responsible for the anomalous normal-state properties and the high- T_c superconductivity [9,10]. However, systematic neutron scattering (NS) and x-ray diffraction (XRD) experiments on the electron doped $\text{BaFe}_{2-x}\text{Ni}_x\text{As}_2$ [11–15] reveal that while T_s and T_N initially decrease with increasing electron doping, their values saturate near optimal superconductivity associated with an incommensurate AF order, resulting in an avoided magnetic QCP [16,17]. In particular, the short-ranged incommensurate AF ordered phase near optimal superconductivity is consistent with a cluster spin glass phase in the matrix of the superconducting phase [18]. Similar conclusions are also reached from muon spin relaxation (μSR) [19] and nuclear magnetic resonance (NMR) measurements [20] on the $\text{BaFe}_{2-x}\text{Co}_x\text{As}_2$ family of materials [21,22], while a separate NMR measurement on $\text{BaFe}_{2-x}\text{Ni}_x\text{As}_2$ suggests the presence of a magnetic QCP at $x = 0.10$ and a structural QCP at $x = 0.14$, both associated with the non-Fermi-liquid behavior [23]. For isovalently doped $\text{BaFe}_2(\text{As}_{1-x}\text{P}_x)_2$, the quantum critical behavior has

been reported near optimal superconductivity around $x = 0.3$ from transport and superfluid density measurements [24–27]. However, recent neutron diffraction measurements show coincident T_s and T_N in the underdoped regime, and the linear extrapolation of the orthorhombic lattice distortion suggests that structural QCP cannot exceed $x = 0.28$ doping [28]. Similarly, it is still unclear if there is a QCP in the hole-doped $\text{Ba}_{1-x}\text{K}_x\text{Fe}_2\text{As}_2$ [29]. To summarize, there is currently no direct evidence demonstrating a gradual suppression of the T_N and T_s to zero temperature with increasing doping inside the superconducting dome. Moreover, it is unclear how magnetism coexists and competes with superconductivity near optimal doping. This is because the occurrence of superconductivity tends to suppress the static AF order and orthorhombic lattice distortion [16,17,19,21,22], thus complicating the ability to determine the intrinsic nature of the AF order without the influence of superconductivity.

One way to determine if there is indeed a magnetic QCP upon suppression of the static AF order is to carry out experiments on materials without superconductivity. For example, transport and neutron powder diffraction experiments on $\text{CeFeAs}_{1-x}\text{P}_x\text{O}$ reveal the presence of a magnetic QCP near $x = 0.4$ without superconductivity that is controlled by the pnictogen height (the average Fe-As/P distance) away from the iron plane [30,31]. Since impurity doping onto the FeAs plane for iron pnictides will suppress superconductivity [32–40], it will be interesting to find a system where one can gradually reduce the AF order with increasing doping but without inducing superconductivity. We have found that Cr impurity doping into $\text{BaFe}_{2-x}\text{Ni}_x\text{As}_2$ is very efficient in suppressing superconductivity without much affecting T_s and T_N of the materials [41]; it would be interesting to carry out neutron scattering NS experiments on these materials to determine the evolution of the structural and magnetic phase transitions in Cr-doped $\text{BaFe}_{2-x}\text{Ni}_x\text{As}_2$ system without the effect of superconductivity.

*These authors made equal contributions to this paper.

†hqluo@iphy.ac.cn

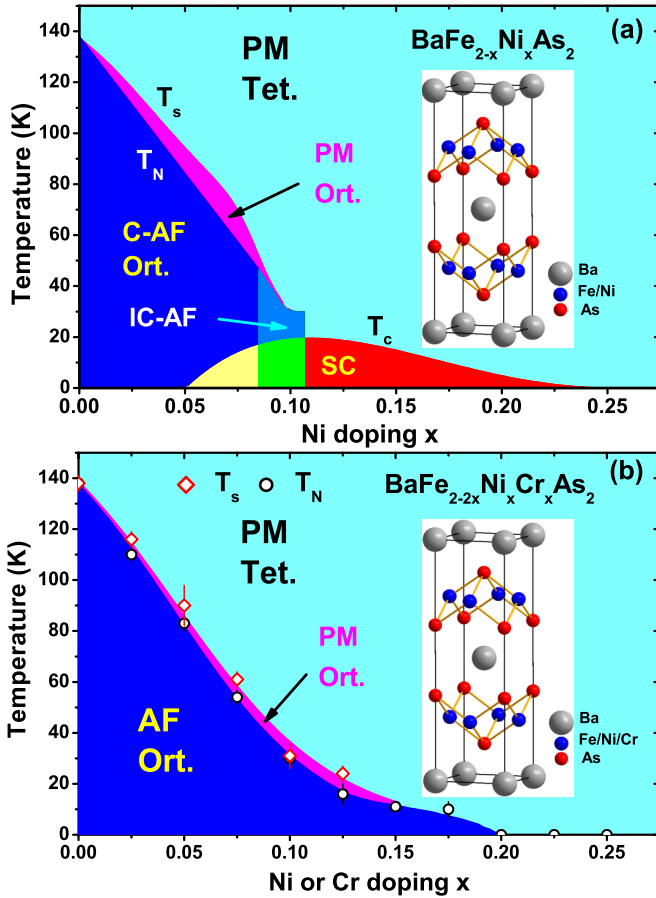


FIG. 1. (Color online) The electronic phase diagram of (a) $\text{BaFe}_{2-x}\text{Ni}_x\text{As}_2$ and (b) $\text{BaFe}_{2-2x}\text{Ni}_x\text{Cr}_x\text{As}_2$. Upon cooling in both systems, a structure transition from tetragonal (Tet.) to orthorhombic (Ort.) lattice and a magnetic transition from paramagnetism (PM) to antiferromagnetism (AF) occur at T_s and T_N , respectively. By approaching the optimal superconductivity around $x = 0.10$ in $\text{BaFe}_{2-x}\text{Ni}_x\text{As}_2$, the long-ranged commensurate antiferromagnetism (C-AF) degenerates into short-ranged incommensurate antiferromagnetism (IC-AF). Inset shows the crystal structure.

In this paper, we report the NS and electric transport studies on the Ni and Cr equivalently doped iron pnictide $\text{BaFe}_{2-2x}\text{Ni}_x\text{Cr}_x\text{As}_2$. Compared with the pure Ni-doped $\text{BaFe}_{2-x}\text{Ni}_x\text{As}_2$ system [Fig. 1(a)] [16–18], we find no evidence for superconductivity while the static AF order is gradually suppressed with increasing equal amounts of Ni and Cr doping [Fig. 1(b)]. For $x \leq 0.10$, T_s and T_N are almost the same as Cr free samples. Upon further increasing x , T_N decreases continuously until it vanishes (within our sensitivity) above $T = 1.5$ K for $x \geq 0.20$. From analysis of the resistivity data at temperatures above T_N , we find no dramatic anomaly for transport behavior around the AF zone boundary $x = 0.20$. Similar resistivity analysis in $\text{BaFe}_{2-x}\text{Ni}_x\text{As}_2$ suggests possible non-Fermi-liquid behavior in the overdoped regime around $x = 0.15$. By fixing Ni composition at $x = 0.30$, increasing Cr doping may significantly affect the transport properties by introducing Kondo or weak localization effects due to impurity scattering, resulting in a possible metal-to-insulator crossover in highly doped $\text{BaFe}_{1.7-y}\text{Ni}_{0.3}\text{Cr}_y\text{As}_2$ ($y \geq 0.30$). Our results

suggest that the non-Fermi-liquid behavior determined from transport measurement is not intimately associated with the disappearance of magnetic order or lattice orthorhombicity, and the impurity scattering is important to the transport properties of iron pnictides.

II. EXPERIMENT

Single crystals of $\text{BaFe}_{2-2x}\text{Ni}_x\text{Cr}_x\text{As}_2$ were grown by self-flux method similar to $\text{BaFe}_{2-x}\text{Ni}_x\text{As}_2$ [41,42]. The in-plane resistivity (ρ_{ab}) was measured by the standard four-probe method in a Quantum Design physical property measurement system. All measured crystals were cut into rectangular shapes $4 \times 0.5 \times 0.1$ mm³ with the c axis being the smallest dimension. Four Ohmic contacts with low resistance (less than 1 Ω) on the ab plane were made by silver epoxy. In order to lower noises, a large current $I = 5$ mA and slow sweeping rate of temperature (2 K/min) were applied. Measurements on each doping were repeated on 3 ~ 5 pieces of crystals to confirm the temperature dependence of $\rho_{ab}(T)$ and reduce uncertainty in estimation of the absolute resistivity due to geometric factors. By directly comparing the temperature dependence of resistivity at different doping concentrations, we normalized the resistivity $\rho_{ab}(T)$ by the data at room temperature ($T = 300$ K).

We carried out elastic neutron scattering experiments using the Rita-2 triple-axis spectrometers at Swiss Spallation Neutron Source, Paul Scherrer Institute, Switzerland. To eliminate the scattering from higher-order neutrons with wavelength λ/n ($n \geq 2$), a pyrolytic graphite (PG) filter before the sample and a cold Be filter after the sample were used. The fixed final energy was $E_f = 4.6$ meV with a wavelength $\lambda_f = 4.2$ Å. The collimation for supermirror guide after the monochromator was $80'$, the radial collimator after the Be filter was about $150'$, and the effective collimation of the neutron-absorbing guide after the analyzer was $40'$ for preventing cross talk between the different detector channels. We also took data on the $x = 0.175, 0.20, 0.25$ compounds using the TAIPAN thermal neutron triple-axis spectrometer at the Bragg Institute, Australian Nuclear Science and Technology Organization (ANSTO). The PG filters were placed before and after the sample. To get better resolution, the PG monochromator and analyzer were set to the flat mode without collimation. The fixed final energy was selected as $E_f = 14.87$ meV ($\lambda_f = 2.3$ Å) or 9.03 meV ($\lambda_f = 3$ Å). We define the wave vector \mathbf{Q} at (q_x, q_y, q_z) as $(H, K, L) = (q_x a / 2\pi, q_y b / 2\pi, q_z c / 2\pi)$ reciprocal lattice units (r.l.u.) using the tetragonal lattice parameters $a \approx b \approx 3.94$ Å, and $c \approx 12.90$ Å. For each experiment, a single crystal with a mass of nearly 1 gram was aligned to the $[H, H, 0] \times [0, 0, L]$ scattering plane. The thickness of our sample is about 0.5 mm, and the neutron absorption is negligible due to small neutron absorption cross sections for all the elements.

III. RESULTS AND DISCUSSION

A. Sample characterization

We first describe the sample characterization of $\text{BaFe}_{2-2x}\text{Ni}_x\text{Cr}_x\text{As}_2$ single crystals. Figure 2(a) shows the XRD patterns on one typical crystal $\text{BaFe}_{1.90}\text{Ni}_{0.05}\text{Cr}_{0.05}\text{As}_2$.

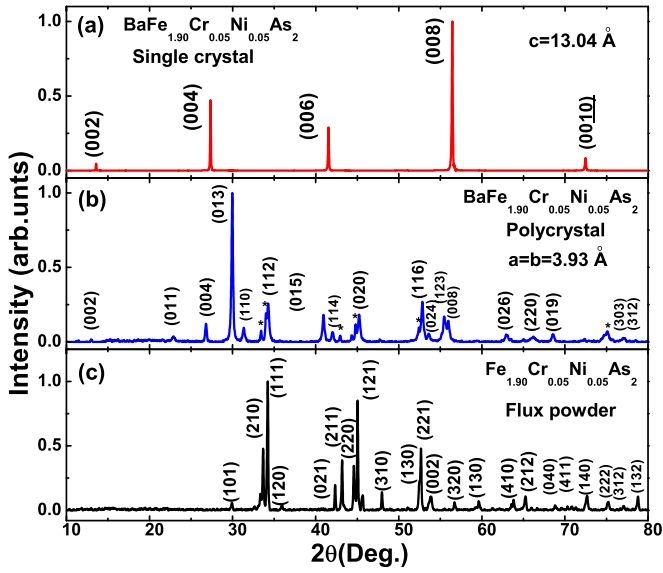


FIG. 2. (Color online) Typical patterns of x-ray diffraction on the (a) as-grown single crystal, (b) polycrystal crushed from single crystal of $\text{BaFe}_{1.9}\text{Ni}_{0.05}\text{Cr}_{0.05}\text{As}_2$, and (c) flux powder of $\text{Fe}_{1.9}\text{Ni}_{0.05}\text{Cr}_{0.05}\text{As}_2$. The stars mark the peaks from residual flux in the crushed crystal. For clarity, the intensity is normalized to $[0, 1]$.

The sharp even peaks $(00l)$ ($l = 2, 4, 6, \dots$) along the c axis with a narrow width of about 0.1° indicate the high crystalline quality of our sample. The calculated c -axis parameter is about 13.04 \AA for this sample, close to the parent compound BaFe_2As_2 . Figure 2(c) shows the XRD results for $\text{Fe}_{1.9}\text{Ni}_{0.05}\text{Cr}_{0.05}\text{As}_2$ powder, which is used as the flux in crystal growth. The powder XRD measurement for crushed crystals (polycrystal) was also carried out to check for possible phase decomposition. As shown in Fig. 2(b), most of the reflections could be indexed to the tetragonal structure with $a = b = 3.93 \text{ \AA}$ at room temperature, except for several small peaks marked by stars from residual flux, which is very common in the self-flux growth method.

To determine the real chemical compositions of our single crystals, we selected several compounds with $x = 0.10, 0.175, 0.20, 0.225, 0.25$ for inductively coupled plasma (ICP) analysis. The segregation coefficient, namely the ratio between real concentration and nominal concentration, $K = C_s/C_l$ for Ni and Cr is about 0.84 and 0.71 in average, respectively, which is consistent with previous reports on $\text{BaFe}_{2-x}\text{Ni}_x\text{As}_2$ [15,41,42]. In order to quantitatively compare with our earlier published results, we simply use the nominal composition to represent all samples in this paper.

B. Antiferromagnetism

The antiferromagnetism was examined by neutron diffraction measurements. Figure 3 shows elastic \mathbf{Q} scans along the $[H, H, 3]$ and $[0.5, 0.5, L]$ directions measured at the Rita-2 triple-axis spectrometer. In order to directly compare the magnetic intensity at each doping level and eliminate the $\lambda/2$ scattering, all data are normalized to 10^4 monitor counts after subtracting the background scattering above T_N . There is no magnetic intensity down to $T = 1.5 \text{ K}$ for the $x = 0.20$

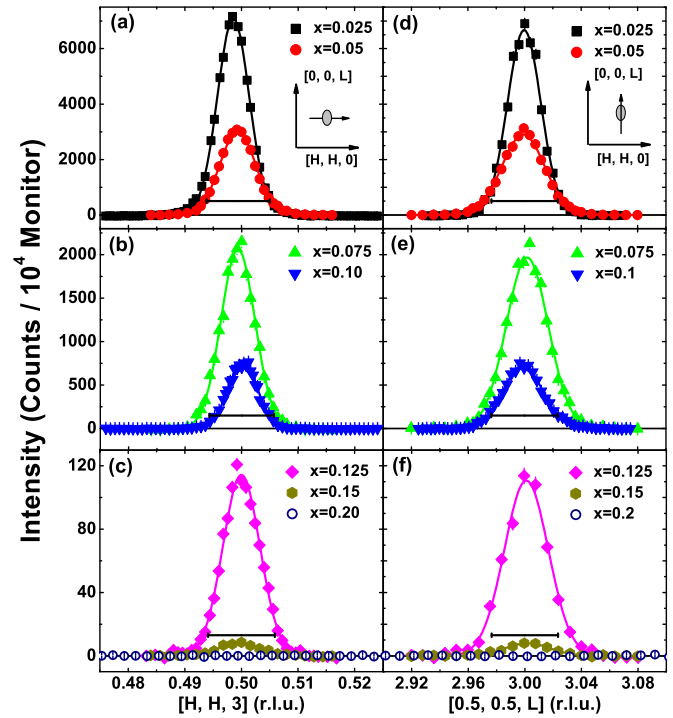


FIG. 3. (Color online) \mathbf{Q} scans for the antiferromagnetic peak at $(0.5, 0.5, 3)$ along (a)–(c) $[H, H, 3]$ and (d)–(f) $[0.5, 0.5, L]$ at 2 K . The black horizontal bars are the instrumental resolution determined by using $\lambda/2$ scattering from the $(1, 1, 6)$ nuclear Bragg peak above T_N without filter. All data are subtracted by the background above T_N . The solid lines are Gaussian fitting results.

compound measured at the TAIPAN triple-axis spectrometer, thus resulting zero net counts for \mathbf{Q} scans [Figs. 3(c) and 3(f)]. The instrumental resolution for the Rita-2 shown as horizontal bars was estimated by using $\lambda/2$ scattering from the $(1, 1, 6)$ nuclear Bragg peak above T_N without a filter, similar to the calculated values of the instrumental resolution ($R_H \sim 0.006 \text{ r.l.u.}$ for $[H, H, 3]$ direction, $R_L \sim 0.024 \text{ r.l.u.}$ for $[0.5, 0.5, L]$ direction) [16]. Although the real instrumental resolution may be slightly larger than these values due to the supermirror guides in the incident beam of the Rita-2 spectrometer, the difference has a negligible effect on samples with different doping levels measured at the same spectrometer. Experimentally, we find that all magnetic peaks shown in Fig. 3 are nearly resolution-limited and exhibit Gaussian distribution similar to the resolution function, suggesting long-ranged magnetic order in this system. The Gaussian fits to the peaks on zero backgrounds are shown by solid lines in Fig. 3 by the function: $I = I_0 \exp[-(H - H_0)^2 / (2\sigma^2)]$ for $[H, H, 3]$ scans, or $I = I_0 \exp[-(L - L_0)^2 / (2\sigma^2)]$ for $[0.5, 0.5, L]$ scans, where the full width at half maximum (FWHM) is $W = 2\sqrt{2} \ln 2 \sigma$ in \AA^{-1} . After the correction from instrument resolution and Fourier transform of the Gaussian peaks from reciprocal space to real space [16,43], we can obtain the spin-spin correlation length $\xi_{ab}^{\text{AF}} = 8 \ln(2) / \sqrt{W_H^2 - R_H^2} / (2\pi\sqrt{2}/a) = 2\sqrt{2} \ln(2) a / (\pi\sqrt{8 \ln(2)\sigma^2 - R_H^2})$ in \AA for in-plane scans along $\mathbf{Q} = [H, H, 3]$, and $\xi_c^{\text{AF}} = 8 \ln(2) / \sqrt{W_L^2 - R_L^2} / (2\pi/c) = 4 \ln(2) c / (\pi\sqrt{8 \ln(2)\sigma^2 - R_L^2})$ in \AA for out-of-plane scans along $\mathbf{Q} = [0.5, 0.5, L]$, where

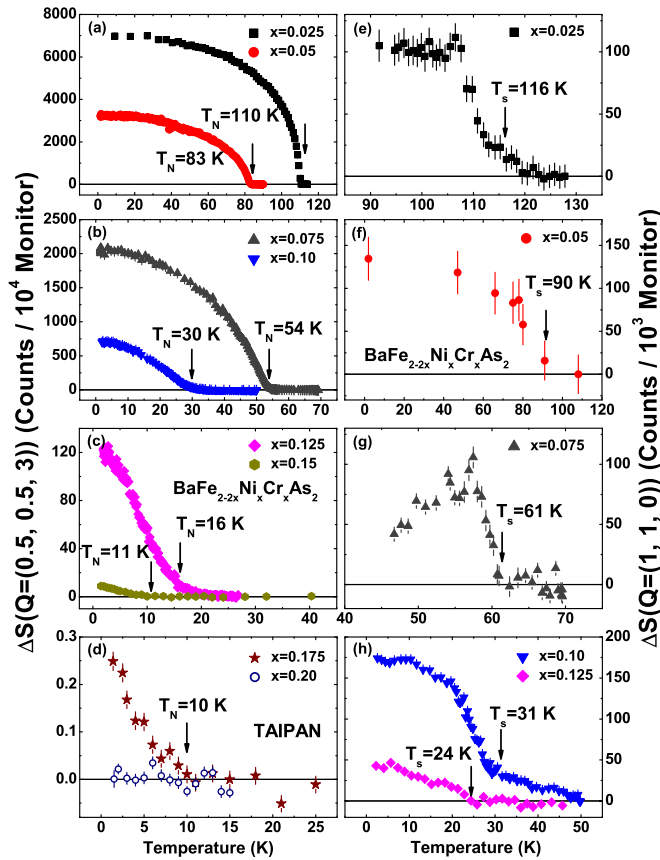


FIG. 4. (Color online) (a)–(d) Order parameter of antiferromagnetism at $Q_{AF} = (0.5, 0.5, 3)$. All data are subtracted by the background above T_N and normalized to 10^4 monitor counts. (e)–(h) Order parameter of structure transition from neutron extinction effect at $Q = (1, 1, 0)$. All data are subtracted by the background above T_s and normalized to 10^3 monitor counts.

the lattice parameters $a \approx b \approx 3.94$ Å, and $c = 12.90$ Å at low temperature. Figure 6(b) presents the doping dependence of spin correlation length in the ab plane ξ_{ab} and along the c axes ξ_c . Clearly, the spin-spin correlations at all doping levels are larger than 400 Å, suggesting the long-ranged nature of the magnetic order. This is different from the $\text{BaFe}_{2-x}\text{Ni}_x\text{As}_2$, where the magnetic order becomes short ranged when $x > 0.08$ before being completely suppressed at $x = 0.108$ [open circles in Fig. 6(b)] [16,17].

The temperature dependence of the intensity at $Q_{AF} = (0.5, 0.5, 3)$ is shown in Figs. 4(a)–4(d), where the Néel temperature T_N is marked by black arrows. For samples with large x where an unambiguous determination of T_N is difficult, we define T_N as the cross point between the linear extrapolations of the decreasing part of the magnetic intensity upon warming and the flat background at high temperature. Here the data are also subtracted by the background above T_N and normalized to 10^4 monitor counts. To determine the possible magnetic order for samples with high doping, we have co-aligned about 12 grams of the $x = 0.20$ and 23 grams of the $x = 0.25$ samples and measured them at the TAIPAN triple-axis spectrometer. After counting about one hour for each temperature from 1.5 to 15 K in 1 K per step at

$Q_{AF} = (0.5, 0.5, 3)$, we find no evidence of static AF order for $x \geq 0.20$ [Fig. 4(d)]. The monotonically increasing intensity below T_N for all magnetically ordered samples suggests that the AF ordered phase is not competing with other phases.

To examine the structure transition temperature T_s , we have measured the temperature dependence of nuclear Bragg reflection at $Q = (1, 1, 0)$. As shown in Figs. 4(e)–4(h), an abrupt jump at T_s arises from the neutron extinction release that occurs due to strain and domain formation related to the orthorhombic distortion [44]. For the $x = 0.10$ sample, we see a clear kink at 31 K corresponding to structure transition. For compounds with $x > 0.125$, the extinction effect becomes unobservable due to much weaker orthorhombic distortion.

In elastic NS, the nuclear peak intensity I_N and magnetic peak intensity I_M are determined by [45]

$$I_N = AN_N(2\pi)^2/V_N \times (|F_N(Q)|)^2/\sin(2\theta_N), \quad (1)$$

and

$$I_M = AN_M(2\pi)^2/V_M \times (|F_M(Q)|)^2/(2\sin(2\theta_M)), \quad (2)$$

where the number of atoms in the magnetic unit cell is $N_M = N_N/2 = 4$, the volume of the magnetic unit cell is $V_M = 2V_N$, and $F_N(Q)$ and $F_M(Q)$ are the structure factor and magnetic form factor at wave vector \mathbf{Q} with scattering angle $2\theta_N$ and $2\theta_M$, respectively. Here we have $F_M(Q) = pS \sum (-1)^l e^{iQd}$, where $p = 0.2659 \times 10^{-12} \text{ cm} \times g \times f_M(Q)$ with $F e^{2+}$ form factor $f_M(Q) = Ae^{aQ^2/16\pi^2} + Be^{bQ^2/16\pi^2} + Ce^{cQ^2/16\pi^2} + D$, S is the magnetic moment along wave vector \mathbf{Q} , d is the spacing of wave vector \mathbf{Q} , and g factor is assumed to be 2. The twinning effect from two kinds of magnetic domains is taken into account in Eq. (2) by dividing the Lorentz factor $|F_M(Q)|^2/\sin(2\theta_M)$ by 2. In principle, by comparing the integrated intensity between the nuclear and magnetic peaks in the form of Eqs. (1) and (2), we can estimate the static magnetic ordered moment via [16,46]

$$S = 0.067 \sqrt{I_M \sin 2\theta_M / I_N \sin 2\theta_N |F_N| / |f_M|}. \quad (3)$$

Several factors have been carefully considered in such an estimation: (1) The neutron absorption may suppress the scattering intensity. In our experiments, we only use one piece of crystal for each measurement, the thickness is about 0.5 mm and almost the same for different dopings. Since our samples do not contain any elements with high neutron absorption, the effect of neutron absorption is negligible. (2) To reduce neutron extinction effect, we use two weak nuclear peaks (1, 1, 0) (structural factor $F_N = 1.31$) and (0, 0, 6) (structural factor $F_N = 8.63$) above T_s for normalizing magnetic peaks at $Q_{AF} = (0.5, 0.5, 1)$ and $(0.5, 0.5, 3)$. (3) To obtain reliable integrated magnetic/nuclear scattering in triple-axis NS experiments [45], we have carried out $\theta - 2\theta$ scans across the Bragg peaks. For samples with small mosaic (our sample mosaic is about $20'$) [42], this is a reliable way to obtain the integrated intensity. We can compare magnetic scattering from different x as most of the experiments are carried out using Rita-2 with identical experimental setup.

Comparing the integrated intensity of magnetic peaks at $Q_{AF} = (0.5, 0.5, 1)$ and $(0.5, 0.5, 3)$ and nuclear peaks at $Q = (1, 1, 0)$ and $(0, 0, 6)$, we estimate the ordered moments for

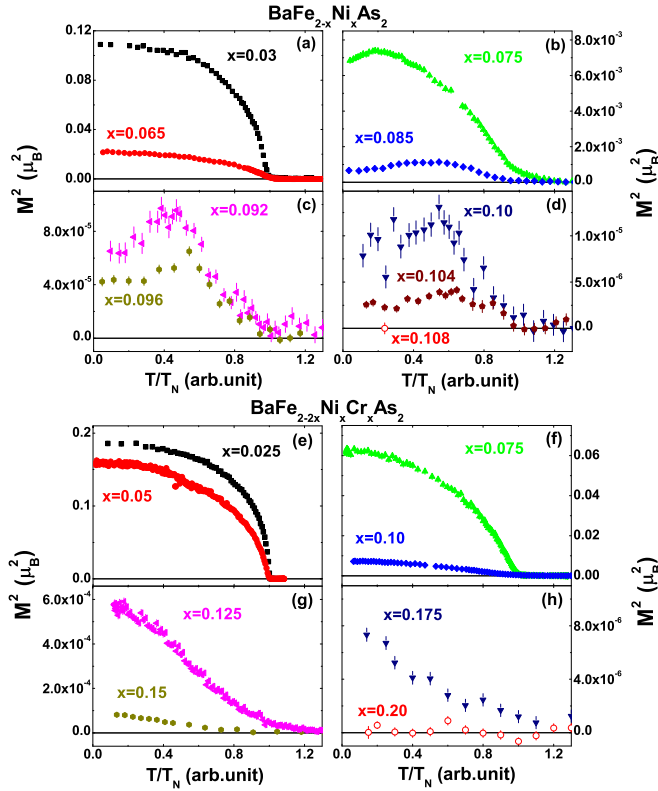


FIG. 5. (Color online) Temperature dependence of the normalized order parameter M^2 vs T/T_N for (a)–(d) $\text{BaFe}_{2-x}\text{Ni}_x\text{As}_2$ and (e)–(h) $\text{BaFe}_{2-2x}\text{Ni}_x\text{Cr}_x\text{As}_2$.

samples with $x = 0.025 - 0.175$ in Fig. 6(a), where the values are taken as the statistical average from different combination of the scattering peaks, and the direction of the ordered moment is simply assumed to be the same as the parent compound BaFe_2As_2 , namely the longitudinal direction $\mathbf{Q} = [H, H, 0]$ for tetragonal lattice [18,47,48]. The Cr doping enhances the magnetic ordered moment compared with those in $\text{BaFe}_{2-x}\text{Ni}_x\text{As}_2$, where the moments are suppressed by superconductivity at low temperatures [16,41]. For high dopings with $x = 0.20$ and 0.25 , the ordered moment M , if it exists, is less than $10^{-3}\mu_B$ at 1.5 K, which is out of the sensitivity of our measurements. The detailed temperature dependence of the ordered moment square M^2 (proportional to order parameters) for both systems is summarized in Fig. 5. The M^2 vs T in both systems behave similarly. The reduction of M^2 in $\text{BaFe}_{2-x}\text{Ni}_x\text{As}_2$ below T_c is due to the effect of superconductivity [16,17], which does not appear in the nonsuperconducting $\text{BaFe}_{2-2x}\text{Ni}_x\text{Cr}_x\text{As}_2$.

Based on the doping dependence of T_s and T_N in this system, we construct the phase diagram of $\text{BaFe}_{2-2x}\text{Ni}_x\text{Cr}_x\text{As}_2$ in Fig. 1(b). For comparison, we also show the phase diagram of $\text{BaFe}_{2-x}\text{Ni}_x\text{As}_2$ in Fig. 1(a). We find that $\text{BaFe}_{2-2x}\text{Ni}_x\text{Cr}_x\text{As}_2$ behaves similarly to Cr free samples for $x \leq 0.10$. However, the long-range AF order still persists for samples with $0.10 \leq x \leq 0.175$ and decreases with increasing x until vanishing around $x = 0.20$. These results are clearly different from the case in $\text{BaFe}_{2-x}\text{Ni}_x\text{As}_2$, where both T_s and T_N saturate around 30 K above optimal $T_c = 20$ K, and the magnetic order disappears in a first order fashion around $x = 0.108$. In addition, the Cr substitution successfully eliminated the

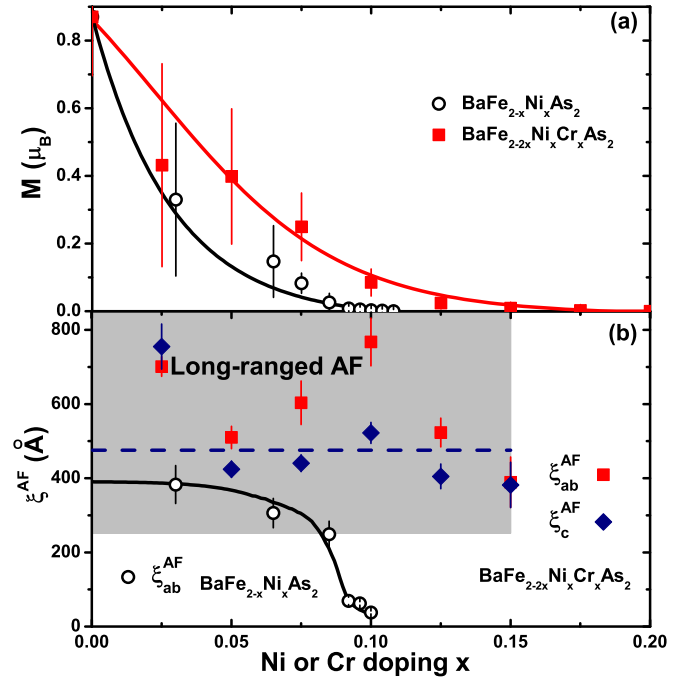


FIG. 6. (Color online) Doping dependence of the (a) ordered moment M and (b) spin-spin correlation length ξ_{AF} in $\text{BaFe}_{2-2x}\text{Ni}_x\text{Cr}_x\text{As}_2$ and $\text{BaFe}_{2-x}\text{Ni}_x\text{As}_2$.

superconducting dome and short-ranged magnetic order in the $\text{BaFe}_{2-x}\text{Ni}_x\text{As}_2$ system, which causes the avoided QCP around optimal superconducting doping $x = 0.10$. These results suggest that Cr doping is an effective way to study magnetism in iron pnictides without the complication of superconductivity.

C. Resistivity

We now discuss the in-plane resistivity measurements for all doping levels of $\text{BaFe}_{2-2x}\text{Ni}_x\text{Cr}_x\text{As}_2$. Figure 7 shows the normalized resistivity $\rho_{ab}(T)/\rho_{ab}(300\text{ K})$ from 2 to 300 K for $x = 0 - 0.30$. No superconductivity is found down to 2 K for all x [41]. The temperature dependence of $\rho_{ab}(T)$ is metallic in the paramagnetic state, and the upturns at low temperatures for lightly doped samples are attributed to the structure and magnetic transition, while the small kink for $x \geq 0.2$ may be from impurity scattering. To fully understand the behavior of $\rho_{ab}(T)$ in the paramagnetic state, we first perform a global fit for the data from $T_s + 20$ to 300 K by the empirical model [16,23,27,49,50]:

$$\rho = \rho_0 + AT^n, \quad (4)$$

where ρ_0 is a constant, A is amplitude, and n is the exponent. Typically, a $n = 2$ power law is expected of a Fermi liquid, while a $n < 2$ power law means non-Fermi-liquid behavior, and a QCP usually corresponds to $n = 1$ as a function of tuning parameter such as doping, pressure, or magnetic field [27,50–52]. In most cases, such fits are performed at low temperature for the domination of electron-electron interactions. However, due to the limited effects on the Debye temperature from Ni or Cr doping less than 15% in the system [53], it is reasonable

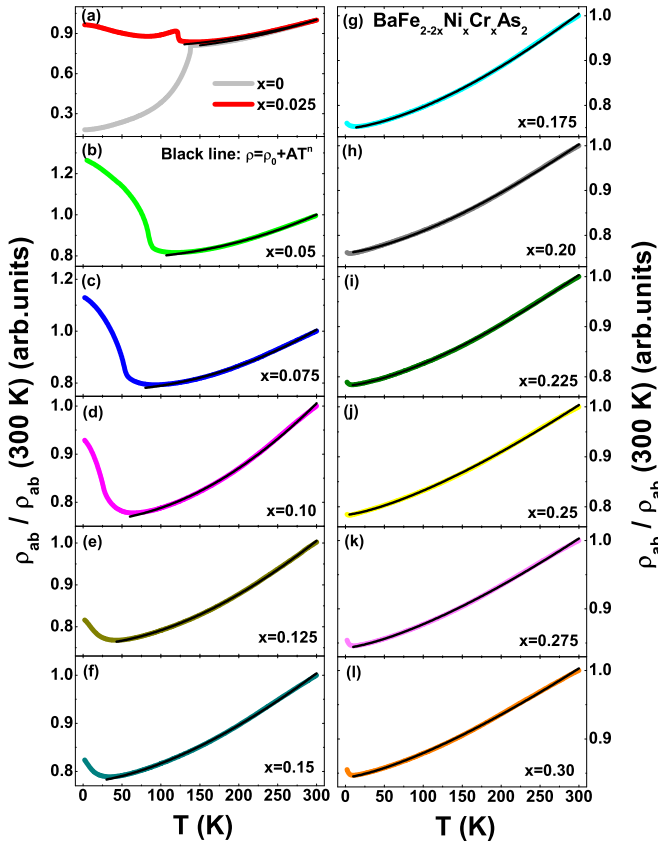


FIG. 7. (Color online) Temperature dependence of in-plane resistivity (normalized by the data at 300 K) for $\text{BaFe}_{2-2x}\text{Ni}_x\text{Cr}_x\text{As}_2$. The black solid lines are global fitting results by the model: $\rho = \rho_0 + AT^n$ up to 300 K in the normal state.

to roughly compare the exponent n up to 300 K for different doping with similar contributions from phonon.

The fitting results are shown in solid black lines in Fig. 7. Similar analysis is also done for the $\text{BaFe}_{2-x}\text{Ni}_x\text{As}_2$ system, as separately shown in Fig. 8, and agree with the original data very well. The exponent n from global fits for different x is summarized in Fig. 9(a). The non-Fermi-liquid behavior with $n < 2$ in $\text{BaFe}_{2-x}\text{Ni}_x\text{As}_2$, occurs above $x = 0.05$, concurrent with the appearance of doping induced superconductivity. The value of n at $x = 0.15$ reduces to about 1.5. Upon doping in $\text{BaFe}_{2-2x}\text{Ni}_x\text{Cr}_x\text{As}_2$, n continuously decreases with increasing x and saturates to around 1.4 for $x \geq 0.20$. Therefore, although the Cr impurities have quite limited effects on T_s and T_N except for suppressing superconductivity, the normal state transport properties are different from pure Ni-doped material. We note that the minimal n in $\text{BaFe}_{2-x}\text{Ni}_x\text{As}_2$ is 1.5 in the overdoped regime, different from the expectation of a standard QCP point. This is consistent with neutron diffraction and XRD results of no QCP near optimal superconductivity [16,17]. Similarly, there is also no dramatic anomaly in n at any doping level of $\text{BaFe}_{2-2x}\text{Ni}_x\text{Cr}_x\text{As}_2$, consistent with the absence of a QCP near $x = 0.20$, even though the T_N of this compound is indeed below 2 K.

To exclude the phonon contributions at high temperatures, an alternative way of analyzing resistivity data is to simply deduce the temperature dependence of n from the slope of the

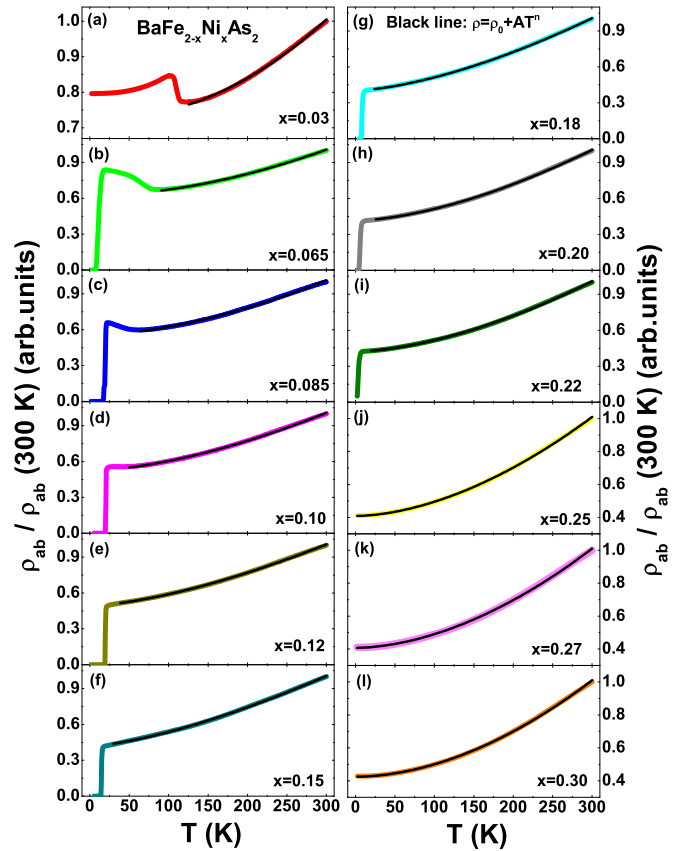


FIG. 8. (Color online) Temperature dependence of in-plane resistivity (normalized by the data at 300 K) for $\text{BaFe}_{2-x}\text{Ni}_x\text{As}_2$. The black solid lines are global fitting results by the model: $\rho = \rho_0 + AT^n$ up to 300 K in the normal state.

curve $\ln(\rho_{ab} - \rho_0)$ as a function of $\ln T$ using Eq. (4). Here the ρ_0 is determined by local fits from $T_s + 20$ K to $T_s + 70$ K. Such a process requires high quality data of $\rho_{ab}(T)$. Figures 9(b) and 9(c) show the temperature and doping dependence of n in the whole phase diagram. The outcome further confirms the global fitting results in Fig. 9(a), where the $n < 2$ behavior mainly exists in $\text{BaFe}_{2-2x}\text{Ni}_x\text{Cr}_x\text{As}_2$ over $x = 0.10$ and in the middle zone with $0.10 \leq x \leq 0.20$ of $\text{BaFe}_{2-x}\text{Ni}_x\text{As}_2$, respectively. We note that the features in Fig. 9(b) are similar to the $\text{BaFe}_2(\text{As}_{1-x}\text{P}_x)_2$ system where the presence of a QCP has been suggested [9], although $\text{BaFe}_{2-x}\text{Ni}_x\text{As}_2$ is in the paramagnetic state above $x = 0.108$ [17].

D. Impurity effect

By successfully eliminating the superconducting dome in $\text{BaFe}_{2-x}\text{Ni}_x\text{As}_2$ via doping equivalent Cr and Ni, we obtain a simple phase diagram in the $\text{BaFe}_{2-2x}\text{Ni}_x\text{Cr}_x\text{As}_2$ system, where the T_N of the material is systematically suppressed to below 2 K around $x = 0.20$. Usually, such a phase diagram would be a strong indication for a magnetic QCP, since the spin correlation length of the AF ordered phase is long ranged for all doping levels. However, the transport properties of the system reveal no anomaly typically associated with a QCP. Future inelastic NS experiments for samples near $x = 0.20$ should be able to determine if energy and temperature are scaled, as is

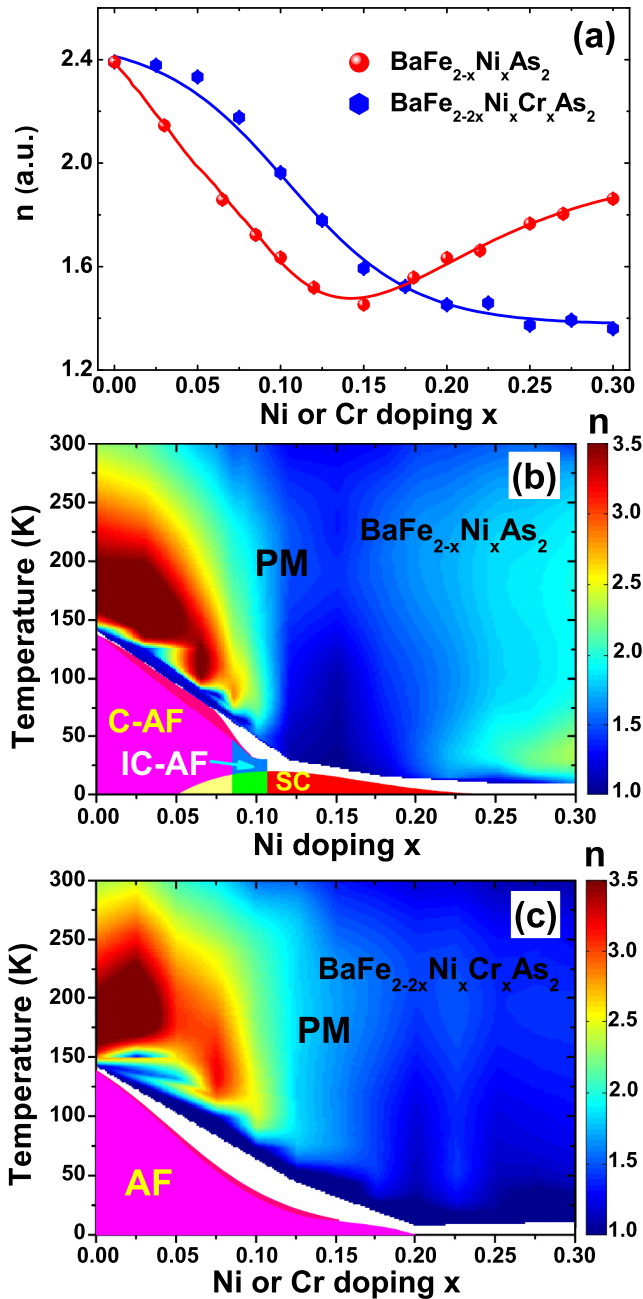


FIG. 9. (Color online) (a) Doping dependence of the exponent n from global fitting results of Figs. 7 and 8. (b) and (c) The gradient color mapping for the temperature and doping dependence of exponent n for $\text{BaFe}_{2-x}\text{Ni}_x\text{As}_2$ and $\text{BaFe}_{2-2x}\text{Ni}_x\text{Cr}_x\text{As}_2$, respectively.

the case for a magnetic QCP [54]. From the results in Figs. 1 and 9, one could argue that the non-Fermi-liquid behavior may not be intimately associated with the disappearance of magnetic order in these systems. On the other hand, for a multiband material such as iron pnictides, it is not clear if transport measurements alone can indeed prove the presence of a QCP. By introducing Cr impurity into $\text{BaFe}_{2-x}\text{Ni}_x\text{As}_2$ to remove superconductivity, the original magnetic phase boundary has been changed possibly due to the impurity effect of Cr doping. Even in the Cr free samples, the Ni doping can cause anisotropic transport properties [55–57].

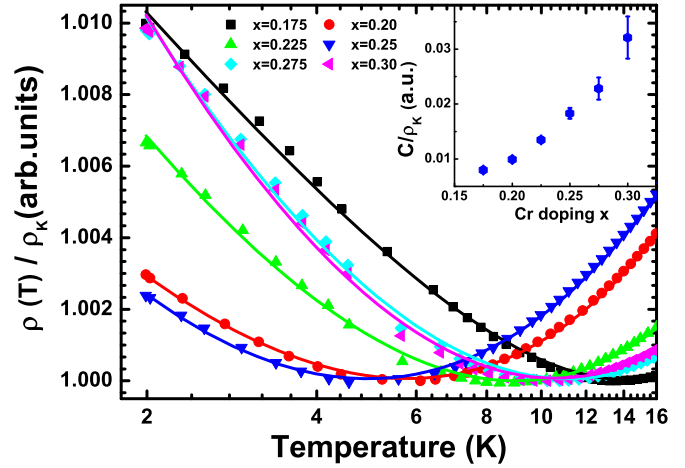


FIG. 10. (Color online) Logarithmic temperature dependence of resistivity for the compounds with $x = 0.175$ – 0.30 . For clarity, all data are normalized by the resistivity at the kink temperature ρ_K . The solid lines are fitting results by Eq. (5).

To better understand the effect of impurity scattering, we note the presence of a small upturn in $\rho_{ab}(T)$ below 10 K even in the highly doped compounds without AF order. Because the Cr ion is magnetic, by doping Cr impurity into a metallic system, additional Kondo scattering may be induced. If this is indeed the case, one may expect a logarithmic dependence of $\rho(T)$ at low temperature, since the temperature dependence of the resistivity including the Kondo effect can be written as: $\rho(T) = \rho_0 + AT^2 + C \ln(T_K/T) + BT^5$, where A , B , and C are constant, and T_K is Kondo temperature [58]. Moreover, a weak localization effect induced by local impurity in the two dimensional electron system may also give rise to a $\ln T$ dependence of resistivity at low temperature [59], which is common in the chemical substituted copper-oxide high temperature superconductors [60]. Interestingly, by plotting the normalized resistivity below 10 K in the logarithmic axis of temperature in Fig. 10, we have found a well defined linear region of $\rho(T)$ as a function of $\ln T$ for $x \geq 0.175$. We then fit the data by the formula:

$$\rho(T) = \rho_0 + AT^n + C \ln(T_K/T), \quad (5)$$

where T_K is fixed as the kink temperature of $\rho_{ab}(T)$, namely, the sign change in temperature of $d\rho_{ab}/dT$. The fitting results as shown by solid lines in Fig. 10 agree very well with the data, and an increase of normalized C/ρ_K upon doping x is found (inset of Fig. 10). Thus the impurity scattering may be proportional to the Cr doping level x . To further confirm this idea, we then fix the Ni concentration as $x = 0.30$ and change Cr from $y = 0$ to $y = 0.8$ in the $\text{BaFe}_{1.7-y}\text{Ni}_{0.3}\text{Cr}_y\text{As}_2$ system. The normalized in-plane resistivity is shown in Figs. 11(a) and 11(b). For small Cr impurity with $y \leq 0.2$, the samples are metallic. Starting from $y = 0.3$, a clear upturn in $\rho_{ab}(T)$ emerges and diverges quickly at low temperatures, finally dominating in the whole temperature range up to 300 K for $y = 0.8$, suggesting a metal-to-insulator crossover in high Cr impurity doped compounds. The color mapping of $d\rho_{ab}/dT$ in Fig. 11(c) confirms this conclusion, where the blue zone marks the negative $d\rho_{ab}/dT$.

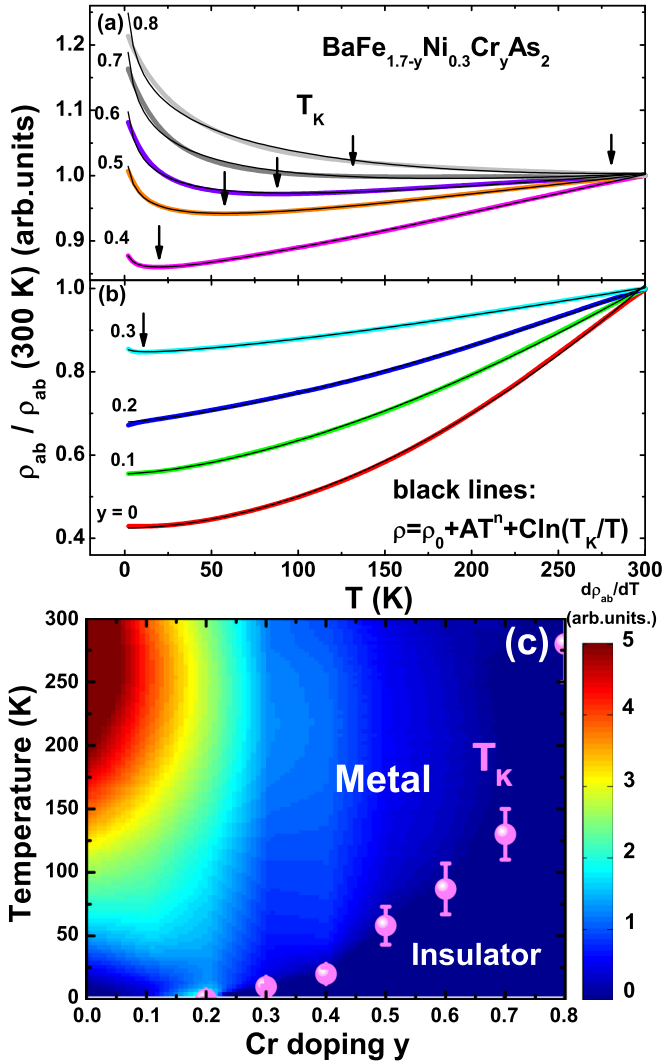


FIG. 11. (Color online) (a) and (b) Temperature dependence of in-plane resistivity for $\text{BaFe}_{1.7-y}\text{Ni}_{0.3}\text{Cr}_y\text{As}_2$ with different Cr doping y . The black solid lines are fitting results by Eq. (5). (c) The gradient color mapping for the temperature and doping dependence of the first order differential of resistivity $d\rho_{ab}/dT$ of $\text{BaFe}_{1.7-y}\text{Ni}_{0.3}\text{Cr}_y\text{As}_2$, where the sign change temperature (kink temperature) T_K marks the zone boundary between the metallic and insulating state.

We also fit the resistivity data using Eq. (5) and obtain the parameters shown in Fig. 12. It seems that C steeply grows up after $x = 0.3$ for strong impurity effects. Surprisingly, the exponent n almost linearly decreases from about 2 to less than 1 and finally increases back to around 2. Such abnormal behaviors are similar to the Cr-free $\text{BaFe}_{2-x}\text{Ni}_x\text{As}_2$ system in a different way of ionic substitutions. Thus it strongly suggests the impurity scattering cannot be ignored in the transport properties in these materials, which may also affect the interpretation of the resistivity data. Therefore, the non-Fermi-liquid feature associated with $n < 2$ may be not a direct evidence for the presence of a magnetic QCP.

IV. CONCLUSIONS

In conclusion, we use elastic neutron scattering and electric transport to study the antiferromagnetic and param-

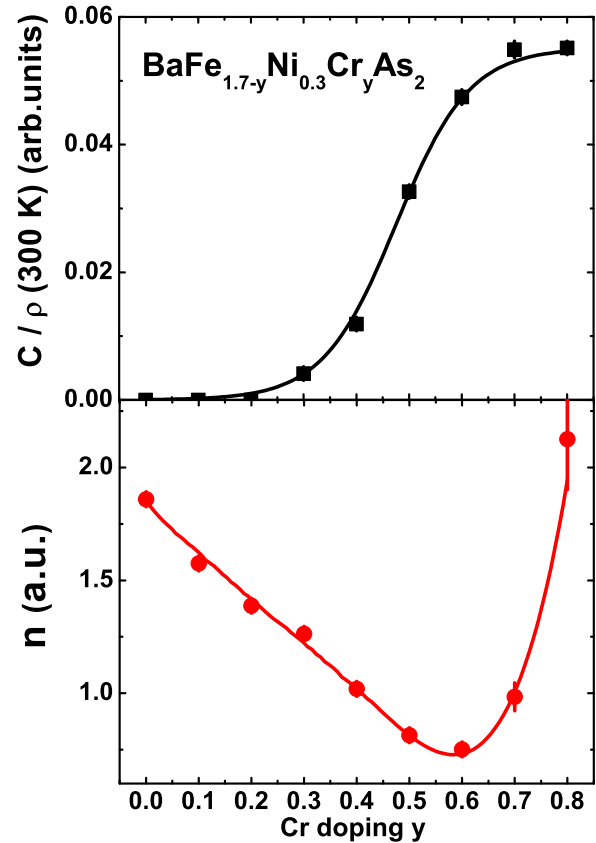


FIG. 12. (Color online) Doping dependence of fitting parameters $C/\rho(300\text{K})$ and n from Fig. 11.

agnetic state behaviors of nonsuperconducting iron pnictide $\text{BaFe}_{2-2x}\text{Ni}_x\text{Cr}_x\text{As}_2$. We find that the long-range AF order terminates at $x = 0.20$ with a systematic decrease of ordered moment and Néel temperature with increasing x . Although the resistivity results suggest non-Fermi-liquid behavior above $x = 0.10$, there is still no direct evidence for a magnetic QCP, while the transport properties are significantly affected by Kondo scattering or weak localization effect from Cr impurity.

ACKNOWLEDGMENTS

The work at IOP, CAS is supported by the National Natural Science Foundation of China (Projects No. 11374011 and No. 91221303), the Ministry of Science and Technology of China (973 projects: 2011CBA00110 and 2012CB821400), and The Strategic Priority Research Program (B) of the Chinese Academy of Sciences (Grant No. XDB07020300). R.Z., X.L. and H.L. acknowledge Project No. 2013DB03 supported by NPL, CAEP. The work at Rice is supported by NSF DMR-1362219, DMR-143606, and the Robert A. Welch Foundation Grant No. C-1839. Part of this work is based on experiments performed at the Swiss spallation neutron source SINQ, Paul Scherrer Institute, Villigen, Switzerland. The authors thank the fruitful discussion with Tao Xiang, and the great help on the crystal growth and characterization from Zhaoyu Liu, Wenliang Zhang, Tao Xie, Lihong Yang, Jun Zhu, Cong Ren, and Xingjiang Zhou.

- [1] P. A. Lee, N. Nagaosa, and X.-G. Wen, *Rev. Mod. Phys.* **78**, 17 (2006).
- [2] D. J. Scalapino, *Rev. Mod. Phys.* **84**, 1383 (2012).
- [3] B. Keimer, S. A. Kivelson, M. R. Norman, S. Uchida, and J. Zaanen, *Nature (London)* **518**, 179 (2015).
- [4] P. Coleman and A. J. Schofield, *Nature (London)* **433**, 226 (2005).
- [5] Y. Kamihara, T. Watanabe, M. Hirano, and H. Hosono, *J. Am. Chem. Soc.* **130**, 3296 (2008).
- [6] C. de la Cruz, Q. Huang, J. W. Lynn, J. Li, W. Ratcliff II, J. L. Zarestky, H. A. Mook, G. F. Chen, J. L. Luo, N. Wang, and P. Dai, *Nature (London)* **453**, 899 (2008).
- [7] G. R. Stewart, *Rev. Mod. Phys.* **83**, 1589 (2011).
- [8] P. Dai, J. Hu, and E. Dagotto, *Nat. Phys.* **8**, 709 (2012).
- [9] T. Shibauchi, A. Carrington, and Y. Matsuda, *Annu. Rev. Condens. Matter Phys.* **5**, 113 (2014).
- [10] J.-H. She, B. J. Overbosch, Y.-W. Sun, Y.-W. Liu, K. E. Schalm, J. A. Mydosh, and J. Zaanen, *Phys. Rev. B* **84**, 144527 (2011).
- [11] M. Rotter, M. Tegel, and D. Johrendt, *Phys. Rev. Lett.* **101**, 107006 (2008).
- [12] A. S. Sefat, R. Jin, M. A. McGuire, B. C. Sales, D. J. Singh, and D. Mandrus, *Phys. Rev. Lett.* **101**, 117004 (2008).
- [13] L. Li, Y. Luo, Q. Wang, H. H. Chen, Z. Ren, Q. Tao, Y. Li, X. Lin, M. He, Z. Zhu, G. Cao, and Z. Xu, *New J. Phys.* **11**, 025008 (2009).
- [14] Q. Huang, Y. Qiu, W. Bao, M. A. Green, J. W. Lynn, Y. C. Gasparovic, T. Wu, G. Wu, and X. H. Chen, *Phys. Rev. Lett.* **101**, 257003 (2008).
- [15] N. Ni, A. Thaler, J. Q. Yan, A. Kracher, E. Colombier, S. L. Bud'ko, P. C. Canfield, and S. T. Hannahs, *Phys. Rev. B* **82**, 024519 (2010).
- [16] H. Luo, R. Zhang, M. Laver, Z. Yamani, M. Wang, X. Lu, M. Wang, Y. Chen, S. Li, S. Chang, J. W. Lynn, and P. Dai, *Phys. Rev. Lett.* **108**, 247002 (2012).
- [17] X. Lu, H. Gretarsson, R. Zhang, X. Liu, H. Luo, W. Tian, M. Laver, Z. Yamani, Y.-J. Kim, A. H. Nevidomskyy, Q. Si, and P. Dai, *Phys. Rev. Lett.* **110**, 257001 (2013).
- [18] X. Lu, D. W. Tam, C. Zhang, H. Luo, M. Wang, R. Zhang, L. W. Harriger, T. Keller, B. Keimer, L.-P. Regnault, T. A. Maier, and P. Dai, *Phys. Rev. B* **90**, 024509 (2014).
- [19] C. Bernhard, C. N. Wang, L. Nuccio, L. Schulz, O. Zaharko, J. Larsen, C. Aristizabal, M. Willis, A. J. Drew, G. D. Varma, T. Wolf, and C. Niedermayer, *Phys. Rev. B* **86**, 184509 (2012).
- [20] A. P. Dioguardi, J. Crocker, A. C. Shockley, C. H. Lin, K. R. Shirer, D. M. Nisson, M. M. Lawson, N. apRoberts-Warren, P. C. Canfield, S. L. Bud'ko, S. Ran, and N. J. Curro, *Phys. Rev. Lett.* **111**, 207201 (2013).
- [21] D. K. Pratt, M. G. Kim, A. Kreyssig, Y. B. Lee, G. S. Tucker, A. Thaler, W. Tian, J. L. Zarestky, S. L. Bud'ko, P. C. Canfield, B. N. Harmon, A. I. Goldman, and R. J. McQueeney, *Phys. Rev. Lett.* **106**, 257001 (2011).
- [22] M. G. Kim, J. Lamsal, T. W. Heitmann, G. S. Tucker, D. K. Pratt, S. N. Khan, Y. B. Lee, A. Alam, A. Thaler, N. Ni, S. Ran, S. L. Bud'ko, K. J. Marty, M. D. Lumsden, P. C. Canfield, B. N. Harmon, D. D. Johnson, A. Kreyssig, R. J. McQueeney, and A. I. Goldman, *Phys. Rev. Lett.* **109**, 167003 (2012).
- [23] R. Zhou, Z. Li, J. Yang, D. Sun, C. Lin, and G. Zheng, *Nat. Commun.* **4**, 2265 (2013).
- [24] K. Hashimoto, K. Cho, T. Shibauchi, S. Kasahara, Y. Mizukami, R. Katsumata, Y. Tsuruhara, T. Terashima, H. Ikeda, M. A. Tanatar, H. Kitano, N. Salovich, R. W. Giannetta, P. Walmsley, A. Carrington, R. Prozorov, and Y. Matsuda, *Science* **336**, 1554 (2012).
- [25] S. Jiang, H. Xing, G. Xuan, CaoWang, Z. Ren, C. Feng, J. Dai, Z. Xu, and G. Cao, *J. Phys.: Condens. Matter* **21**, 382203 (2009).
- [26] S. Kasahara, T. Shibauchi, K. Hashimoto, K. Ikada, S. Tonegawa, R. Okazaki, H. Shishido, H. Ikeda, H. Takeya, K. Hirata, T. Terashima, and Y. Matsuda, *Phys. Rev. B* **81**, 184519 (2010).
- [27] J. G. Analytis, H. Kuo, R. D. McDonald, M. Wartenbe, P. M. C. Rourke, N. E. Hussey, and I. R. Fisher, *Nat. Phys.* **10**, 194 (2014).
- [28] J. M. Allred, K. M. Taddei, D. E. Bugaris, S. Avci, D. Y. Chung, H. Claus, C. dela Cruz, M. G. Kanatzidis, S. Rosenkranz, R. Osborn, and O. Chmaissem, *Phys. Rev. B* **90**, 104513 (2014).
- [29] S. Avci, O. Chmaissem, D. Y. Chung, S. Rosenkranz, E. A. Goremychkin, J. P. Castellán, I. S. Todorov, J. A. Schlueter, H. Claus, A. Daoud-Aladine, D. D. Khalyavin, M. G. Kanatzidis, and R. Osborn, *Phys. Rev. B* **85**, 184507 (2012).
- [30] C. de la Cruz, W. Z. Hu, S. Li, Q. Huang, J. W. Lynn, M. A. Green, G. Chen, N. L. Wang, H. A. Mook, Q. Si, and P. Dai, *Phys. Rev. Lett.* **104**, 017204 (2010).
- [31] Y. Luo, Y. Li, S. Jiang, J. Dai, G. Cao, and Z. A. Xu, *Phys. Rev. B* **81**, 134422 (2010).
- [32] P. Cheng, B. Shen, J. Hu, and H.-H. Wen, *Phys. Rev. B* **81**, 174529 (2010).
- [33] Y. F. Guo, Y. G. Shi, S. Yu, A. A. Belik, Y. Matsushita, M. Tanaka, Y. Katsuya, K. Kobayashi, I. Nowik, I. Felner, V. P. S. Awana, K. Yamaura, and E. Takayama-Muromach, *Phys. Rev. B* **82**, 054506 (2010).
- [34] J. Li, Y. Guo, S. Zhang, S. Yu, Y. Tsujimoto, H. Kontani, K. Yamaura, and E. Takayama-Muromachi, *Phys. Rev. B* **84**, 020513(R) (2011).
- [35] J. Li, Y. F. Guo, S. B. Zhang, J. Yuan, Y. Tsujimoto, X. Wang, C. I. Sathish, Y. Sun, S. Yu, W. Yi, K. Yamaura, E. Takayama-Muromachiu, Y. Shirako, M. Akaogi, and H. Kontani, *Phys. Rev. B* **85**, 214509 (2012).
- [36] J. Li, J. Yuan, M. Ji, G. Zhang, J.-Y. Ge, H.-L. Feng, Y.-H. Yuan, T. Hatano, W. Hu, K. Jin, T. Schwarz, R. Kleiner, D. Koelle, K. Yamaura, H.-B. Wang, P.-H. Wu, E. Takayama-Muromachi, J. Vanacken, and V. V. Moshchalkov, *Phys. Rev. B* **90**, 024512 (2014).
- [37] P. Cheng, B. Shen, F. Han, and H. Wen, *Europhys. Lett.* **104**, 37007 (2013).
- [38] Y. Li, C. Shen, Y. Luo, X. Yang, Q. Tao, G. Cao, and Z. Xu, *Europhys. Lett.* **102**, 37003 (2013).
- [39] T. Inabe, T. Kawamata, T. Noji, T. Adachi, and Y. Koike, *J. Phys. Soc. Jap.* **82**, 044712 (2013).
- [40] Q. Deng, X. Ding, S. Li, J. Tao, H. Yang, and H. Wen, *New J. Phys.* **16**, 063020 (2014).
- [41] R. Zhang, D. Gong, X. Lu, S. Li, P. Dai, and H. Luo, *Supercond. Sci. Technol.* **27**, 115003 (2014).
- [42] Y. Chen, X. Lu, M. Wang, H. Luo, and S. Li, *Supercond. Sci. Technol.* **24**, 065004 (2011).
- [43] H. J. Kang, P. Dai, H. A. Mook, D. N. Argyriou, V. Sikolenko, J. W. Lynn, Y. Kurita, S. Komiya, and Y. Ando, *Phys. Rev. B* **71**, 214512 (2005).
- [44] X. Lu, J. T. Park, R. Zhang, H. Luo, A. H. Nevidomskyy, Q. Si, and P. Dai, *Science* **345**, 657 (2014).

- [45] G. Shirane, S. M. Shapiro, and J. M. Tranquada, *Neutron Scattering with a Triple-Axis Spectrometer* (Cambridge University Press, Cambridge, 2004).
- [46] S. Li, C. de la Cruz, Q. Huang, G. F. Chen, T.-L. Xia, J. L. Luo, N. L. Wang, and P. Dai, *Phys. Rev. B* **80**, 020504(R) (2009).
- [47] S. D. Wilson, Z. Yamani, C. R. Rotundu, B. Freelon, E. Bourret-Courchesne, and R. J. Birgeneau, *Phys. Rev. B* **79**, 184519 (2009).
- [48] N. Qureshi, P. Steffens, S. Wurmehl, S. Aswartham, B. Behner, and M. Braden, *Phys. Rev. B* **86**, 060410(R) (2012).
- [49] A. Rosch, *Phys. Rev. Lett.* **82**, 4280 (1999).
- [50] Y. Luo, L. Pourovskii, S. E. Rowley, Y. Li, C. Feng, A. Georges, J. Dai, G. Cao, Z. Xu, Q. Si, and N. P. Ong, *Nat. Mater.* **13**, 777 (2014).
- [51] R. A. Cooper, *Science* **323**, 603 (2009).
- [52] H. v. Löhneysen, A. Rosch, M. Vojta, and P. Wölfle, *Rev. Mod. Phys.* **79**, 1015 (2007).
- [53] B. Zeng, B. Shen, H. Luo, G. Mu, P. Cheng, H. Yang, L. Shan, C. Ren, and H.-H. Wen, *Phys. Rev. B* **85**, 224514 (2012).
- [54] A. Schröder, G. Aeppli, R. Coldea, M. Adams, O. Stockert, H. v. Löhneysen, E. Bucher, R. Ramazashvili, and P. Coleman, *Nature (London)* **407**, 351 (2000).
- [55] A. E. Böhmer, P. Burger, F. Hardy, T. Wolf, P. Schweiss, R. Fromknecht, M. Reinecker, W. Schranz, and C. Meingast, *Phys. Rev. Lett.* **112**, 047001 (2014).
- [56] S. Ishida, M. Nakajima, T. Liang, K. Kihou, C. H. Lee, A. Iyo, H. Eisaki, T. Kakeshita, Y. Tomioka, T. Ito, and S. Uchida, *Phys. Rev. Lett.* **110**, 207001 (2013).
- [57] M. P. Allan, T.-M. Chuang, F. Massee, Y. Xie, N. Ni, S. L. Bud'ko, G. S. Boebinger, Q. Wang, D. S. Dessau, P. C. Canfield, M. S. Golden, and J. C. Davis, *Nat. Phys.* **9**, 220 (2013).
- [58] J. Kondo, *Prog. Theor. Phys.* **32**, 37 (1964).
- [59] P. A. Lee and T. V. Ramakrishnan, *Rev. Mod. Phys.* **57**, 287 (1985).
- [60] H. Luo and H.-H. Wen, *Phys. Rev. B* **89**, 024506 (2014).